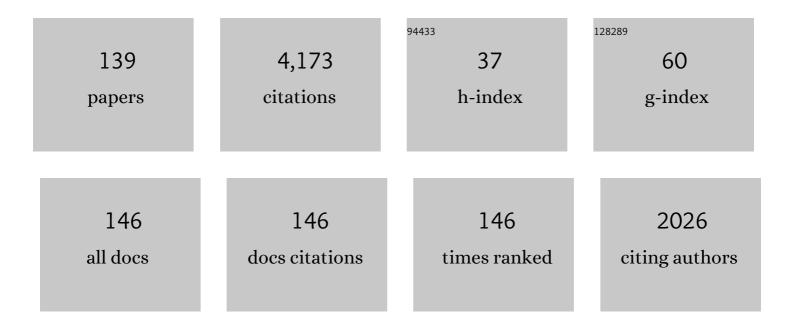
List of Publications by Year in descending order

Source: https://exaly.com/author-pdf/7353788/publications.pdf Version: 2024-02-01



#	Article	IF	CITATIONS
1	Burning plasma achieved in inertial fusion. Nature, 2022, 601, 542-548.	27.8	233
2	Fusion Energy Output Greater than the Kinetic Energy of an Imploding Shell at the National Ignition Facility. Physical Review Letters, 2018, 120, 245003.	7.8	205
3	Microtesla MRI of the human brain combined with MEG. Journal of Magnetic Resonance, 2008, 194, 115-120.	2.1	159
4	Inertially confined fusion plasmas dominated by alpha-particle self-heating. Nature Physics, 2016, 12, 800-806.	16.7	144
5	First High-Convergence Cryogenic Implosion in a Near-Vacuum Hohlraum. Physical Review Letters, 2015, 114, 175001.	7.8	117
6	The neutron imaging diagnostic at NIF (invited). Review of Scientific Instruments, 2012, 83, 10D317.	1.3	116
7	Symmetry control of an indirectly driven high-density-carbon implosion at high convergence and high velocity. Physics of Plasmas, 2017, 24, .	1.9	106
8	Demonstration of High Performance in Layered Deuterium-Tritium Capsule Implosions in Uranium Hohlraums at the National Ignition Facility. Physical Review Letters, 2015, 115, 055001.	7.8	101
9	The high velocity, high adiabat, "Bigfoot―campaign and tests of indirect-drive implosion scaling. Physics of Plasmas, 2018, 25, .	1.9	90
10	MRI with an atomic magnetometer suitable for practical imaging applications. Journal of Magnetic Resonance, 2009, 199, 188-191.	2.1	89
11	SQUID detected NMR in microtesla magnetic fields. Journal of Magnetic Resonance, 2004, 170, 1-7.	2.1	87
12	Design of inertial fusion implosions reaching the burning plasma regime. Nature Physics, 2022, 18, 251-258.	16.7	87
13	High-Performance Indirect-Drive Cryogenic Implosions at High Adiabat on the National Ignition Facility. Physical Review Letters, 2018, 121, 135001.	7.8	86
14	Spatio-temporal mapping of rat whisker barrels with fast scattered light signals. NeuroImage, 2005, 26, 619-627.	4.2	85
15	SQUID-based instrumentation for ultralow-field MRI. Superconductor Science and Technology, 2007, 20, S367-S373.	3.5	85
16	Approaching a burning plasma on the NIF. Physics of Plasmas, 2019, 26, .	1.9	83
17	Neutron source reconstruction from pinhole imaging at National Ignition Facility. Review of Scientific Instruments, 2014, 85, 023508.	1.3	78
18	Toward direct neural current imaging by resonant mechanisms at ultra-low field. NeuroImage, 2008, 39. 310-317.	4.2	76

#	Article	IF	CITATIONS
19	Simultaneous magnetoencephalography and SQUID detected nuclear MR in microtesla magnetic fields. Magnetic Resonance in Medicine, 2004, 52, 467-470.	3.0	68
20	SQUIDs in biomagnetism: a roadmap towards improved healthcare. Superconductor Science and Technology, 2016, 29, 113001.	3.5	67
21	Parallel MRI at microtesla fields. Journal of Magnetic Resonance, 2008, 192, 197-208.	2.1	65
22	Nuclear imaging of the fuel assembly in ignition experiments. Physics of Plasmas, 2013, 20, 056320.	1.9	65
23	Improved Performance of High Areal Density Indirect Drive Implosions at the National Ignition Facility using a Four-Shock Adiabat Shaped Drive. Physical Review Letters, 2015, 115, 105001.	7.8	58
24	Impact of Localized Radiative Loss on Inertial Confinement Fusion Implosions. Physical Review Letters, 2020, 124, 145001.	7.8	58
25	Thin Shell, High Velocity Inertial Confinement Fusion Implosions on the National Ignition Facility. Physical Review Letters, 2015, 114, 145004.	7.8	56
26	Co-Registration of Interleaved MEG and ULF MRI Using a 7 Channel Low-\$T_{m c}\$ SQUID System. IEEE Transactions on Applied Superconductivity, 2011, 21, 456-460.	1.7	55
27	Achieving record hot spot energies with large HDC implosions on NIF in HYBRID-E. Physics of Plasmas, 2021, 28, .	1.9	55
28	Ultra-low-field MRI for the detection of liquid explosives. Superconductor Science and Technology, 2010, 23, 034023.	3.5	53
29	Toward a burning plasma state using diamond ablator inertially confined fusion (ICF) implosions on the National Ignition Facility (NIF). Plasma Physics and Controlled Fusion, 2019, 61, 014023.	2.1	53
30	SQUID-Based Microtesla MRI for In Vivo Relaxometry of the Human Brain. IEEE Transactions on Applied Superconductivity, 2009, 19, 823-826.	1.7	50
31	Hotspot conditions achieved in inertial confinement fusion experiments on the National Ignition Facility. Physics of Plasmas, 2020, 27, .	1.9	50
32	2015, 22, 056314.	1.9	49
33	The role of hot spot mix in the low-foot and high-foot implosions on the NIF. Physics of Plasmas, 2017, 24, .	1.9	49
34	SQUID-detected ultra-low field MRI. Journal of Magnetic Resonance, 2013, 229, 127-141.	2.1	47
35	On concomitant gradients in low-field MRI. Journal of Magnetic Resonance, 2005, 175, 103-113.	2.1	46
36	Hot-spot mix in large-scale HDC implosions at NIF. Physics of Plasmas, 2020, 27, .	1.9	46

#	Article	IF	CITATIONS
37	Multi-Channel SQUID System for MEG and Ultra-Low-Field MRI. IEEE Transactions on Applied Superconductivity, 2007, 17, 839-842.	1.7	45
38	Progress of indirect drive inertial confinement fusion in the United States. Nuclear Fusion, 2019, 59, 112018.	3.5	38
39	SQUID-Based Simultaneous Detection of NMR and Biomagnetic Signals at Ultra-Low Magnetic Fields. IEEE Transactions on Applied Superconductivity, 2005, 15, 635-639.	1.7	33
40	Neutron imaging with the short-pulse laser driven neutron source at the Trident laser facility. Journal of Applied Physics, 2016, 120, .	2.5	32
41	Plasma stopping-power measurements reveal transition from non-degenerate to degenerate plasmas. Nature Physics, 2020, 16, 432-437.	16.7	28
42	Experimental results of radiation-driven, layered deuterium-tritium implosions with adiabat-shaped drives at the National Ignition Facility. Physics of Plasmas, 2016, 23, .	1.9	27
43	Three-dimensional reconstruction of neutron, gamma-ray, and x-ray sources using spherical harmonic decomposition. Journal of Applied Physics, 2017, 122, .	2.5	27
44	Time-Resolved Fuel Density Profiles of the Stagnation Phase of Indirect-Drive Inertial Confinement Implosions. Physical Review Letters, 2020, 125, 155003.	7.8	27
45	Progress Toward a Deployable SQUID-Based Ultra-Low Field MRI System for Anatomical Imaging. IEEE Transactions on Applied Superconductivity, 2015, 25, 1-5.	1.7	26
46	Implosion performance of subscale beryllium capsules on the NIF. Physics of Plasmas, 2019, 26, 052707.	1.9	26
47	SQUIDs vs. Induction Coils for Ultra-Low Field Nuclear Magnetic Resonance: Experimental and Simulation Comparison. IEEE Transactions on Applied Superconductivity, 2011, 21, 465-468.	1.7	25
48	Hotspot parameter scaling with velocity and yield for high-adiabat layered implosions at the National Ignition Facility. Physical Review E, 2020, 102, 023210.	2.1	25
49	Instrumentation for Simultaneous Detection of Low Field NMR and Biomagnetic Signals. IEEE Transactions on Applied Superconductivity, 2005, 15, 676-679.	1.7	24
50	Fluence-compensated down-scattered neutron imaging using the neutron imaging system at the National Ignition Facility. Review of Scientific Instruments, 2016, 87, 11E715.	1.3	24
51	Probabilistic forward model for electroencephalography source analysis. Physics in Medicine and Biology, 2007, 52, 5309-5327.	3.0	23
52	Applications of Ultra-Low Field Magnetic Resonance for Imaging and Materials Studies. IEEE Transactions on Applied Superconductivity, 2009, 19, 835-838.	1.7	23
53	Noise-free magnetoencephalography recordings of brain function. Physics in Medicine and Biology, 2004, 49, 2117-2128.	3.0	22
54	Non-cryogenic anatomical imaging in ultra-low field regime: Hand MRI demonstration. Journal of Magnetic Resonance, 2011, 211, 101-108.	2.1	22

#	Article	IF	CITATIONS
55	SQUID-based systems for co-registration of ultra-low field nuclear magnetic resonance images and magnetoencephalography. Physica C: Superconductivity and Its Applications, 2012, 482, 19-26.	1.2	22
56	Integrated performance of large HDC-capsule implosions on the National Ignition Facility. Physics of Plasmas, 2020, 27, .	1.9	22
57	Mix and hydrodynamic instabilities on NIF. Journal of Instrumentation, 2017, 12, C06001-C06001.	1.2	21
58	Ultra-low field NMR measurements of liquids and gases with short relaxation times. Journal of Magnetic Resonance, 2006, 183, 134-141.	2.1	20
59	On three-dimensional reconstruction of a neutron/x-ray source from very few two-dimensional projections. Journal of Applied Physics, 2015, 118, .	2.5	20
60	Achieving 280 Gbar hot spot pressure in DT-layered CH capsule implosions at the National Ignition Facility. Physics of Plasmas, 2020, 27, .	1.9	20
61	Observation of Hydrodynamic Flows in Imploding Fusion Plasmas on the National Ignition Facility. Physical Review Letters, 2021, 127, 125001.	7.8	20
62	Performance of a novel SQUID-based superconducting imaging-surface magnetoencephalography system. Physica C: Superconductivity and Its Applications, 2002, 368, 18-23.	1.2	18
63	Progress on Detection of Liquid Explosives Using Ultra-Low Field MRI. IEEE Transactions on Applied Superconductivity, 2011, 21, 530-533.	1.7	16
64	Simultaneous usage of pinhole and penumbral apertures for imaging small scale neutron sources from inertial confinement fusion experiments. Review of Scientific Instruments, 2012, 83, 10D316.	1.3	16
65	Combined neutron and x-ray imaging at the National Ignition Facility (invited). Review of Scientific Instruments, 2016, 87, 11D703.	1.3	15
66	Variable convergence liquid layer implosions on the National Ignition Facility. Physics of Plasmas, 2018, 25, .	1.9	15
67	Density determination of the thermonuclear fuel region in inertial confinement fusion implosions. Journal of Applied Physics, 2020, 127, .	2.5	15
68	Self characterization of a coded aperture array for neutron source imaging. Review of Scientific Instruments, 2014, 85, 123506.	1.3	14
69	Design of the polar neutron-imaging aperture for use at the National Ignition Facility. Review of Scientific Instruments, 2016, 87, 11D821.	1.3	13
70	Demonstration of transmission high energy electron microscopy. Applied Physics Letters, 2018, 112, .	3.3	13
71	Simulations of indirectly driven gas-filled capsules at the National Ignition Facility. Physics of Plasmas, 2014, 21, .	1.9	12
72	A liquid VI scintillator cell for fast-gated neutron imaging. Review of Scientific Instruments, 2018, 89, 101142.	1.3	12

#	Article	IF	CITATIONS
73	Deficiencies in compression and yield in x-ray-driven implosions. Physics of Plasmas, 2020, 27, .	1.9	12
74	Three dimensional low-mode areal-density non-uniformities in indirect-drive implosions at the National Ignition Facility. Physics of Plasmas, 2021, 28, .	1.9	12
75	Fill tube dynamics in inertial confinement fusion implosions with high density carbon ablators. Physics of Plasmas, 2020, 27, .	1.9	11
76	Three-dimensional reconstruction of neutron, gamma-ray, and x-ray sources using a cylindrical-harmonics expansion. Review of Scientific Instruments, 2021, 92, 033508.	1.3	11
77	Fuel convergence sensitivity in indirect drive implosions. Physics of Plasmas, 2021, 28, 042705.	1.9	11
78	Experiments to explore the influence of pulse shaping at the National Ignition Facility. Physics of Plasmas, 2020, 27, 112708.	1.9	11
79	First-Order Planar Superconducting Quantum Interference Device Gradiometers With Long Baseline. IEEE Transactions on Applied Superconductivity, 2007, 17, 672-675.	1.7	10
80	Demonstration of a time-integrated short line of sight neutron imaging system for inertial confinement fusion. Review of Scientific Instruments, 2015, 86, 125112.	1.3	10
81	Toward SQUID-Based Direct Measurement of Neural Currents by Nuclear Magnetic Resonance. IEEE Transactions on Applied Superconductivity, 2007, 17, 854-857.	1.7	9
82	Optimization and Configuration of SQUID Sensor Arrays for a MEG-MRI System. IEEE Transactions on Applied Superconductivity, 2013, 23, 1601304-1601304.	1.7	9
83	Aperture design for the third neutron and first gamma-ray imaging systems for the National Ignition Facility. Review of Scientific Instruments, 2018, 89, 10127.	1.3	9
84	First D+D neutron image at the National Ignition Facility. Physics of Plasmas, 2018, 25, .	1.9	9
85	Ultra-Low Field NMR of \${m UF}_{6}\$ for \$^{235}{m U}\$ Detection and Characterization. IEEE Transactions on Applied Superconductivity, 2009, 19, 816-818.	1.7	8
86	Noise Modeling From Conductive Shields Using Kirchhoff Equations. IEEE Transactions on Applied Superconductivity, 2011, 21, 489-492.	1.7	8
87	Simultaneous neutron and x-ray imaging of inertial confinement fusion experiments along a single line of sight at Omega. Review of Scientific Instruments, 2015, 86, 043503.	1.3	8
88	Magnetic Resonance Relaxometry at Low and Ultra Low Fields. IFMBE Proceedings, 2010, 28, 82-87.	0.3	8
89	Toward High Resolution Images With SQUID-Based Ultra-Low Field Magnetic Resonance Imaging. IEEE Transactions on Applied Superconductivity, 2013, 23, 1603107-1603107.	1.7	7
90	First downscattered neutron images from Inertial Confinement Fusion experiments at the National Ignition Facility. EPJ Web of Conferences, 2013, 59, 13018.	0.3	7

#	Article	IF	CITATIONS
91	Toward early cancer detection using superparamagnetic relaxometry in a SQUID-based ULF-MRI system. Superconductor Science and Technology, 2014, 27, 044031.	3.5	7
92	Results from neutron imaging of ICF experiments at NIF. Journal of Physics: Conference Series, 2016, 688, 012064.	0.4	7
93	Principal factors in performance of indirect-drive laser fusion experiments. Physics of Plasmas, 2020, 27, .	1.9	7
94	Measurements of enhanced performance in an indirect drive inertial confinement fusion experiment when reducing the contact area of the capsule support. Physics of Plasmas, 2020, 27, .	1.9	7
95	SQUIDs for Magnetic Resonance Imaging at Ultra-low Magnetic Field. Progress in Electromagnetics Research Symposium: [proceedings] Progress in Electromagnetics Research Symposium, 2009, 5, 466-470.	0.4	7
96	Summary of the first neutron image data collected at the National Ignition Facility. EPJ Web of Conferences, 2013, 59, 13017.	0.3	6
97	A concept to collect neutron and x-ray images on the same line of sight at NIF. Review of Scientific Instruments, 2014, 85, 11E614.	1.3	6
98	Optimizing neutron imaging line of sight locations for maximizing sampling of the cold fuel density in inertial confinement fusion implosions at the National Ignition Facility. Review of Scientific Instruments, 2018, 89, 101147.	1.3	6
99	Source Localization Precision of the Superconducting Imaging-Surface MEG System. Biomedizinische Technik, 2001, 46, 38-40.	0.8	5
100	Detection of 3He spins with ultra-low field nuclear magnetic resonance employing SQUIDs for application to a neutron electric dipole moment experiment. Journal of Magnetic Resonance, 2008, 195, 129-133.	2.1	5
101	A new aperture for neutron and x-ray imaging of inertial confinement fusion experiments. Review of Scientific Instruments, 2012, 83, 10E522.	1.3	5
102	Polarization enhancement technique for nuclear quadrupole resonance detection. Solid State Nuclear Magnetic Resonance, 2014, 61-62, 35-38.	2.3	5
103	Toward 3D data visualization using virtual reality tools. Review of Scientific Instruments, 2021, 92, 033528.	1.3	5
104	Three-dimensional diagnostics and measurements of inertial confinement fusion plasmas. Review of Scientific Instruments, 2021, 92, 053526.	1.3	5
105	First graded metal pushered single shell capsule implosions on the National Ignition Facility. Physics of Plasmas, 2022, 29, .	1.9	4
106	Hydroscaling indirect-drive implosions on the National Ignition Facility. Physics of Plasmas, 2022, 29, .	1.9	4
107	Determining x-ray spectra of radiographic sources with a Compton spectrometer. Proceedings of SPIE, 2014, , .	0.8	3
108	Measuring x-ray spectra of flash radiographic sources. Proceedings of SPIE, 2015, , .	0.8	3

#	Article	IF	CITATIONS
109	Nuclear Diagnostics at the National Ignition Facility, 2013-2015. Journal of Physics: Conference Series, 2016, 717, 012117.	0.4	3
110	A wide-acceptance Compton spectrometer for spectral characterization of a medical x-ray source. Proceedings of SPIE, 2016, , .	0.8	3
111	Design of the aperture array for neutron imaging from the north pole of the National Ignition Facility. Proceedings of SPIE, 2016, , .	0.8	3
112	System design of the NIF Neutron Imaging System North Pole. , 2017, , .		3
113	Three-dimensional characterization of the third line-of-site neutron imaging pinhole at NIF. , 2019, , .		3
114	Using ultra-low field nuclear magnetic resonance for direct neural current measurements. International Congress Series, 2007, 1300, 582-585.	0.2	2
115	Multi-sensor system for simultaneous ultra-low-field MRI and MEG. International Congress Series, 2007, 1300, 631-634.	0.2	2
116	Multi-axis neutron imaging at the National Ignition Facility. Proceedings of SPIE, 2015, , .	0.8	2
117	Solid polystyrene and deuterated polystyrene light output response to fast neutrons. Review of Scientific Instruments, 2016, 87, 043513.	1.3	2
118	Calibration of two compact permanent magnet spectrometers for high current electron linear induction accelerators. Review of Scientific Instruments, 2018, 89, 073303.	1.3	2
119	Spectral characterization of flash and high flux x-ray radiographic sources with a magnetic Compton spectrometer. Review of Scientific Instruments, 2021, 92, 083102.	1.3	2
120	Bound on hot-spot mix in high-velocity, high-adiabat direct-drive cryogenic implosions based on comparison of absolute x-ray and neutron yields. Physical Review E, 2022, 106, .	2.1	2
121	IMAGING MAGNETIC SOURCES IN THE PRESENCE OF SUPERCONDUCTING SURFACES: MODEL & EXPERIMENT. Biomedizinische Technik, 2001, 46, 159-161.	0.8	1
122	Radiation damping for speedingâ€up NMR applications. Concepts in Magnetic Resonance Part A: Bridging Education and Research, 2012, 40A, 179-185.	0.5	1
123	The neutron imaging system fielded at the National Ignition Facility. EPJ Web of Conferences, 2013, 59, 13016.	0.3	1
124	Lens design challenges for scintillator-based neutron imaging. , 2018, , .		1
125	Evolution of the neutron imaging aperture. , 2018, , .		1
126	Experimental investigation of high temperature superconducting imaging surface magnetometry. Review of Scientific Instruments, 2002, 73, 2360-2363.	1.3	0

#	Article	IF	CITATIONS
127	Forward model theoretical basis for a superconducting imaging surface magnetoencephalography system. Physics in Medicine and Biology, 2004, 49, 523-532.	3.0	0
128	Performance characteristics of the neutron imaging diagnostic at NIF. , 2011, , .		0
129	On a ghost artefact in ultra low field magnetic resonance relaxation imaging. Journal of Magnetic Resonance, 2014, 243, 98-106.	2.1	0
130	Multi-Channel SQUID-Based Ultra-Low Field Magnetic Resonance Imaging in Unshielded Environment. , 2015, , .		0
131	Overview of Performance and Progress with Inertially Confined Fusion Implosions on the National Ignition Facility. , 2015, , .		0
132	Scintillator Characterization Measurements for Neutron Imaging in Inertial Confinement Fusion. , 2017, , .		0
133	Demonstration of transmission high energy electron microscopy. AIP Conference Proceedings, 2020, ,	0.4	0
134	MagViz: A Bottled Liquids Scanner Using Ultra-Low Field NMR Relaxometry. NATO Science for Peace and Security Series B: Physics and Biophysics, 2014, , 99-110.	0.3	0
135	Electric and Magnetic Fields of the Brain. , 2014, , 73-105.		0
136	CHAPTER 7. Detection Using SQUIDs and Atomic Magnetometers. New Developments in NMR, 2015, , 183-224.	0.1	0
137	Electric and Magnetic Fields of the Brain. , 2019, , 111-143.		0
138	Electric and Magnetic Fields of the Brain. , 2019, , 1-33.		0
139	Bootstrap estimation of the effect of instrument response function uncertainty on the reconstruction of fusion neutron sources. Review of Scientific Instruments, 2022, 93, 043508.	1.3	0